INTERNATIONAL JOURNAL OF HYDROGEN ENERGY 46 (2021) 7573–7588

Available online at www.sciencedirect.com

ScienceDirect

journal homepage: www.elsevier.com/locate/he

# Effect of syngas fuel compositions on the occurrence of instability of laminar diffusion flame

*Tananop Piemsinlapakunchon, Manosh C. Paul**

*Systems, Power & Energy Research Division, James Watt School of Engineering, University of Glasgow, Glasgow, G12 8QQ, United Kingdom*

## HIGHLIGHTS

- Instability of laminar diffusion flame of syngas reported.
- Impacts of chemical compositions of syngas on instability elucidated.
- $H_2$ in syngas significantly increases flame temperature and fluctuation.
- $CH_4$ further increases instability and heat fluctuation.
- Flame of 25%$H_2$+75%CO reported the best performance.

## ARTICLE INFO

*Article history:*
Received 2 October 2020
Received in revised form
13 November 2020
Accepted 28 November 2020
Available online 24 December 2020

*Keywords:*
Syngas combustion
Diffusion flame instability
Combustion modelling
Heat generation
Flame characteristics

## ABSTRACT

The paper presents a numerical investigation of the critical roles played by the chemical compositions of syngas on laminar diffusion flame instabilities. Three different flame phenomena – stable, flickering and tip-cutting – are formulated by varying the syngas fuel rate from 0.2 to 1.4 SLPM. Following the satisfactory validation of numerical results with Darabkhani et al. [1], the study explored the consequence of each species ($H_2$, CO, $CH_4$, $CO_2$, $N_2$) in the syngas composition. It is found that low $H_2$:CO has a higher level of instability, which however does not rise any further when the ratio is less than 1. Interestingly, CO encourages the heat generation with less fluctuation while $H_2$ plays another significant role in the increase of flame temperature and its fluctuation. Diluting $CH_4$ into syngas further increases the instability level as well as the fluctuation of heat generation significantly. However, an opposite effect is found from the same action with either $CO_2$ or $N_2$. Finally, considering the heat generation and flame stability, the highest performance is obtained from 25%$H_2$+75%CO (81 W), followed by EQ+20%$CO_2$, and EQ+20%$N_2$ (78 W).



## Introduction

An increase in the demand for energy worldwide encourages the research and development towards the production and utilisation of clean and sustainable energy [2]. Syngas, defined as the mixture of hydrogen ($H_2$) and carbon monoxide (CO), is one of the promising options in this respect ([3,4]). It could be produced from various forms of feedstock such as food waste, biomass waste, coal, and agricultural waste [5–9], and [10]. However, this benefit has an impact on the diversity it

* *Corresponding author.*
E-mail address: Manosh.Paul@glasgow.ac.uk (M.C. Paul).
https://doi.org/10.1016/j.ijhydene.2020.11.259

presents in its fuel compositions. Depending on the production process and feedstock, syngas contains not only $H_2$ and CO but also methane ($CH_4$), carbon dioxide ($CO_2$), nitrogen ($N_2$) and other impurities at various percentages ([8–11]). Therefore, the design of a combustion system that is suitable for the diverse syngas is challenging. Inevitably, a microscopic understanding of the combustion characteristics to be affected by the diversity in syngas composition is fundamentally important for utilising this gas fuel effectively.

In the recent years, the characteristics of syngas diffusion flame have been studied in the several papers. This flame type being the energy source is also used in various applications at different scales, e.g. in industrial furnace, cooking hob, and external combustion chamber. The fundamental of this flame type in which the fuel and oxidiser streams are supplied into combustion separately is also similar to combustion in a gas turbine engine. A diffusion flame could also be categorised based on the flow regime of fuel stream as laminar or turbulent ([12–17], and [18]). These studies principally focused on the investigation of impact of syngas composition on the flame temperature, flame appearance, heat release, and emission.

The knowledge gap is identified from the review of literature for the flame condition when the fuel and oxidiser are supplied at an improper ratio that has the potential to destabilise the flame movement to cause instability such as 'flickering' and 'tip-cutting'. The difference between the phenomena of stable, flickering, and tip-cutting flames are illustrated in Fig. 1. Briefly, a flickering flame – as presented in the figure – only moves upward and downward forming an oscillative cycle, while its tip is cut at the body when it is a tip-cutting flame. Due to this, the instability level of a tip-cutting flame will be higher than that of a flickering flame. Both these phenomena were studied in the several pieces of published literature for the diffusion flames of methane ($CH_4$), propane ($C_3H_8$), mixture of both species ($CH_4$+$C_8H_8$), and hydrogen [19]. However, as reported in our earlier work that the diversity of syngas composition strongly affects the stable diffusion flame characteristics [20]. Thus, the composition is expected to play a significant role in the flame instability and this paper for the first time addresses this issue.

An in-depth understanding of flame instability is crucially important since this phenomenon directly affects the performance and consistency of the heat generation of flame. This work aims to fulfil the scientific knowledge gap by critically examining the impacts of the syngas fuel compositions on the instability of a buoyancy drive laminar diffusion flame. Also, the impact of these phenomena on the flame temperature and heat generation capability is particularly focused. Further, attention is paid on the flickering and tip-cutting phenomena with the influence of the variation of the flow rates of both fuel and co-flow air. The co-flow burner of [21] which was designed specifically for studying the tip-cutting and the flickering flame is modelled numerically in this paper. The validation of newly generated model is firstly presented, followed by the study of the impact of syngas composition on flame instabilities.

## Model formulation

Detailed geometry of the co-flow burner modelled in the paper was already presented in Darabkhani and Zhang of [21]. In brief, the inner diameter of the fuel and co-flow air tube of the burner is 4.57 and 37.8 mm respectively, whereas the position of the co-flow air exit is 4 mm lower than the fuel exit. The

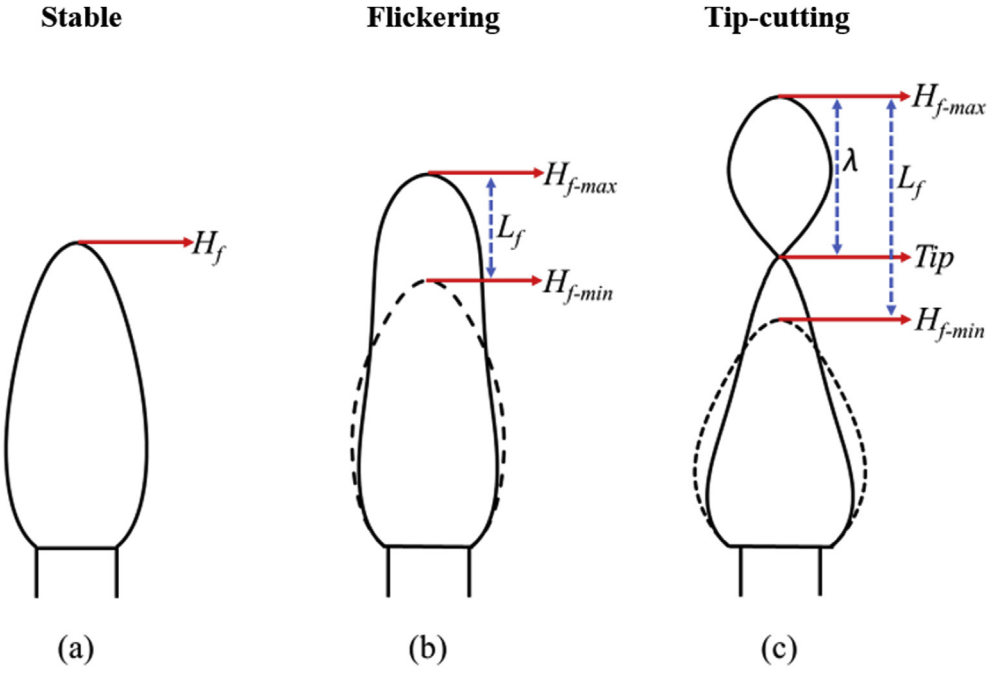


**Fig. 1 – Illustration of stable, flickering, and tip-cutting flames with related parameters.**

shape of the fuel inlet tube is a tapered nozzle which assists the stabilisation of flame.

The burner is modelled by creating an axisymmetric domain according to the stated geometrical design, and presented in Fig. 2. The domain covers the volume above the fuel and air exit, with the height and width extended to 204 mm and 32.9 mm, respectively. It is worth noting that the symmetric axis is on the right-hand side of the domain.

The fuel and co-flow air inlets, at the bottom of the domain, are both defined as a velocity inlet. The top and left-hand sides of the boundary are both assinged a pressure boundary where the temperature and pressure are set to 293 K and 1 atm respectively. The species on these boundaries are air with a composition consisting of 79% $N_2$ and 21% $O_2$. Lastly, the fuel and air tubes are defined as a no-slip wall boundary.

The generated mesh, as illustrated in Fig. 2, is designed particularly considering the interaction and chemical reactions to occur between the fuel and co-flow air streams, and also between the fuel/air stream and the fuel/air tube. The higher density zone, therefore, locates at the edge of the fuel and air tubes. The non-uniform mesh is developed by a hyperbolic function stretching from the smallest cell to the highest one. In the validation stage, the mesh dependency test is also performed considering three different levels of mesh resolution. The fine, medium and coarse mesh resolutions have the smallest cell size of 1.25E-4, 2E-4, and 3.33E-4 respectively, with the corresponding cell numbers of 39,560, 19,720, and 6720. Among them, the mesh level providing a good comparative result with a reasonable computational cost will be selected for the study stage.

## Governing equations and numerical techniques

The numerical simulation employed is transient, thus the time step for each simulation case is computed based on the convective courant number, which is set as 1. The governing equations for the axisymmetric domain are presented below [22,23]:

*Continuity equation*

$$\frac{\partial \rho}{\partial t}+\frac{\partial(\rho u_x)}{\partial x}+\frac{\partial(\rho u_r)}{\partial r}+\frac{\rho u_r}{u_r}=0 \tag{1}$$

*Momentum equation*

$$\frac{\partial(\rho u_x)}{\partial t}+\frac{1}{r}\frac{\partial(r\rho u_x u_x)}{\partial x}+\frac{1}{r}\frac{\partial(r\rho u_r u_x)}{\partial r}=-\frac{\partial p}{\partial x}+\frac{1}{r}\frac{\partial}{\partial x}\left[r\mu\left(2\frac{\partial u_r}{\partial x}-\frac{2}{3}(\nabla\cdot\vec{u})\right)\times\right]+\frac{1}{r}\frac{\partial}{\partial r}\left[r\mu\left(\frac{\partial u_x}{\partial r}-\frac{\partial u_r}{\partial x}\right)\right]+\rho g_x \tag{2}$$

$$\frac{\partial(\rho u_r)}{\partial t}+\frac{1}{r}\frac{\partial(r\rho u_x u_r)}{\partial x}+\frac{1}{r}\frac{\partial(r\rho u_r u_r)}{\partial r}=-\frac{\partial p}{\partial r}+\frac{1}{r}\frac{\partial}{\partial x}\left[r\mu\left(\frac{\partial u_r}{\partial x}-\frac{\partial u_x}{\partial r}\right)\times\right]+\frac{1}{r}\frac{\partial}{\partial r}\left[r\mu\left(2\frac{\partial u_r}{\partial r}-\frac{2}{3}(\nabla\cdot\vec{u})\right)\right]-2\mu\frac{u_r}{r^2}+\frac{2}{3}\frac{\mu}{r}(\nabla\cdot\vec{u}) \tag{3}$$

where $u$ is the velocity component ($ms^{-1}$), $t$ is the time, $\rho$ is the mixture density,$x$ is the axial coordinate, $r$ is the radial coordinate, the subscription $x$ and $r$ refers to the direction,$\mu$ is the dynamic viscosity, $p$ is the static pressure, and $\rho g_x$ is the gravitational body force. The term $\nabla\cdot\vec{u}$ is expressed as:

$$\nabla\cdot\vec{u}=\frac{\partial(\rho u_x)}{\partial x}+\frac{\partial(\rho u_r)}{\partial r}+\frac{\rho u_r}{u_r} \tag{4}$$

*Species transport equation*

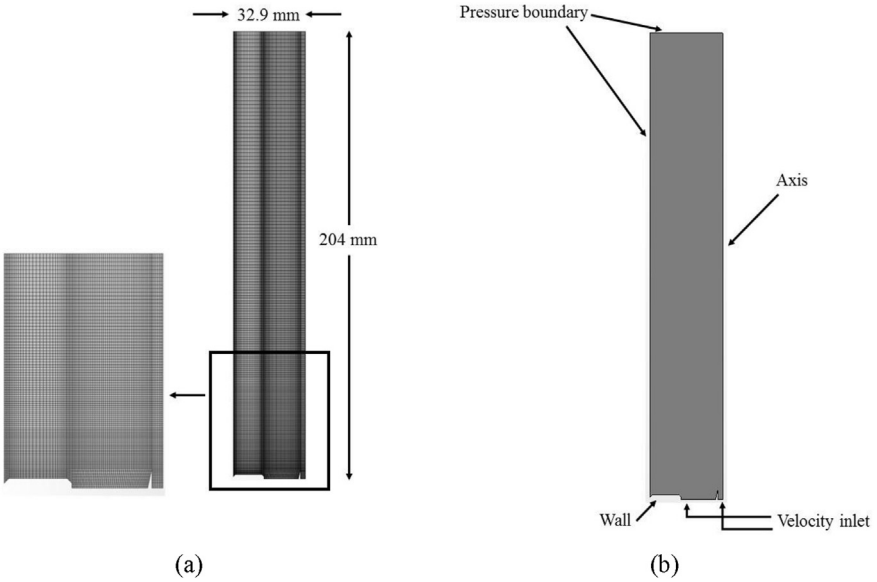


**Fig. 2 – (a) Mesh generation and (b) boundary conditions of a simulation domain.**

$$\frac{\partial}{\partial t}(\rho Y_i) + \nabla \cdot (\rho Y_i \vec{u} + J_i) = R_i \quad (5)$$

where $R_i$ is the production rate of species i, $J_i$ is the diffusive heat flux which relates to the molecular diffusion and thermal diffusion, and $Y_i$ is the mass fraction of species i. The expression of $J_i$ is defined according to the Fick's law as

$$J_i = \rho D_i (\nabla \cdot Y_i) + \rho \frac{D_{i,t}}{T}(\nabla \cdot T) \quad (6)$$

where $D_i$ is the molecular diffusivity coefficient of species i, $D_{i,t}$ is the thermal diffusion coefficient for species i.

*Energy transport equation*

$$\frac{\partial}{\partial t}(\rho E) + \nabla \cdot \left(\vec{u}(\rho E + p) = -\left(\nabla \cdot q_j\right) + Q_r\right) \quad (7)$$

where $q_j$ is the energy flux, and $Q_r$ is the thermal energy production rate. The total energy ($E$) is computed based on the enthalpy ($h$) of the mixture as

$$h = E + \frac{p}{\rho} \quad (8)$$

The dynamic viscosity ($\mu$) of the mixture is the combination of the same definition of each individual species based on their mass fraction. At the species level, the dynamic viscosity ($\mu_i$) of species $i$ is defined by interpolating the gas property data for the major species such as $H_2$, CO, $CH_4$, $CO_2$, $N_2$, $O_2$, and $H_2O$ with a constant value for the other species [22]. The thermal conductivity ($\lambda t$) is computed according to the kinetic theory for an individual species then combined with the method proposed by Mathur-Saxena [23]. It considers the translation contribution ($C_{v,tran}$), rotation contribution ($C_{v,rot}$) and vibration contribution ($C_{v,vib}$) as follows:

$$\lambda t_i = \frac{\mu_i}{M_i}\left(f_{tran} C_{v,tran} + f_{rot} C_{v,rot} + f_{vib} C_{v,vib}\right) \quad (9)$$

$$\lambda t_{mix} = \frac{1}{2}\left(\sum_1^n X_i \varnothing_i + \left(\sum_1^n \frac{X_i}{\lambda t_i}\right)^{-1}\right) \quad (10)$$

The model considers the thermal radiation, and its transport equation is solved by the Discrete Ordinates Method (DOM) [24]. The radiative property e.g. absorption coefficient is calculated by the weighted sum of gray gas model (WSGG), in which the species $H_2O$ and $CO_2$ are assumed to dominate the cloud emission and absorption. According to the setup of the simulation domain, the medium is assumed to be optically thin, and the combustion product gases ($H_2O$, $CO_2$ and $N_2$) occupy the majority of the volume. The optical path length ($S$) supplied into the WSGG model is calculated as

$$S = 3.6 \frac{Volume\ of\ the\ domain}{surfacce\ area\ of\ domain} \quad (11)$$

Further, the transient segregated implicit unsteady solver is selected for solving the continuity, momentum, species, and energy equations with the boundary conditions described in the previous sections. An inbuilt algorithm 'operator splitting' in STAR CCM + CFD software is also utilised for formulating the species transport equation, and the details of this algorithm are available in Ref. [24]. The DRM22 [25] chemical mechanism, which consists of 22 species and 104 chemical reactions is imported to the model for processing the reaction pathway of each species. This chemical reaction mechanism is capable of predicting the combustion of syngas with the reasonable result comparing to the experimental one [26]. The sundials CVODE ODE solver, developed and introduced by Ref. [27], is selected for computing the reaction rates and chemical reactions.

The ignition is set to occur at the area above the fuel tube. The cells around this area are set to have a temperature of 1800 K for the first 0.5s to trigger the combustion. The time step is defined according to the convective courant number ((CCN)) as

$$CCN = \Delta t\left(\frac{cell\ velocity}{\Delta x}\right) \quad (12)$$

The maximum value of *CCN* is monitored at every time-step, and this parameter is maintained at 1 ± 0.05 by increasing or decreasing the time-step through a user-defined function (UDF). The cell having the smallest size (an area close to the fuel tube) is found to have the maximum value of *CCN* while the value is 30–50% lower at the reaction zone of the flame. By applying this setup, the time-step is adjusted automatically by UDF which becomes stable once the maximum *CCN* satisfies the preferable range.

## Data extraction

According to the study of [1], the analysis to be performed relates to the several important parameters, e.g. (i) the magnitude of flame oscillation ($L_f$), (ii) the oscillation wavelength ($\lambda$), and (iii) the average oscillating flame height ($H_f$-*ave*). The parameters $L_f$ and $\lambda$ are already illustrated in Fig. 1, where $L_f$ is defined as the difference between the maximum and minimum flame height ($H_f$-*max* - $H_f$-*min*); and $\lambda$ is the difference between $H_f$-*max* and tip-cutting position. Further, $H_f$-*ave* is calculated from the average flame height during an instability cycle (($H_f$-*min* + $H_f$-*max*)/2). Thus, according to this, there are three parameters to be required for processing the simulation datasets: $H_f$-*max*, $H_f$-*min*, and tip-cutting position. Further, the values of $L_f$ and λ are greater than zero for a tip-cutting flame, whereas a flickering flame has the value of $L_f > 0$ and $\lambda = 0$, and a stable flame has both $L_f$ and $\lambda$ equalling to zero.

The flame front line, where the stoichiometric combustion occurs, is drawn by a zero-temperature gradient method introduced by Ref. [16]. The position where the flame front line crosses the axis represents the flame height ($H_f$). The value of $H_f$ is monitored and plotted every time-step, and this action forms the profile of this parameter changing over time, and the instability cycle is observed from this profile. The value of $L_f$, $\lambda$ and $H_f$-*ave* are consequently calculated from the profile. Three different types of profile are obtained from the stable, flickering, and tip-cutting flames, and the values of $H_f$-*max*, $H_f$-*min*, and tip-cutting are extracted as presented in Fig. 3.

The same approach i.e. the average flame length ($H_f$-*ave*) is also applied for the flame temperature ($T$) and the total chemistry heat release ($Q$). These parameters are, therefore,

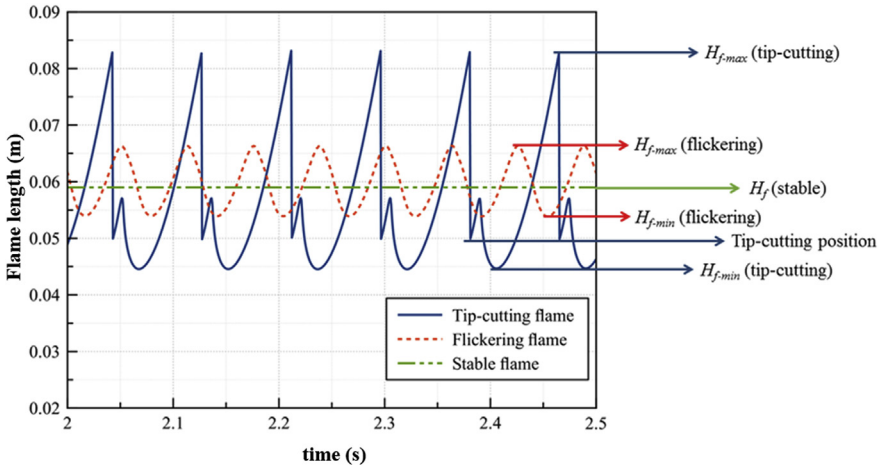


**Fig. 3 – Description of the various flame length profiles over time.**

monitored at every time-step and subsequently, their profiles and changes over the time are extracted for the respective maximum and minimum values to finally compute the average flame temperature (*T-ave*) and the total chemistry heat release (*Q-ave*). By the same principle as $L_f$, which is the difference between the maximum and minimum value, the fluctuations in *T* and *Q* are examined.

## Validation of the generated model

The combustion condition and experimental results of Darabkhani et al. [1] are used as a reference at this stage, and accordingly the flame of $CH_4$ is formulated at the fuel rate of 0.2–0.35 SLPM (standard litre per minute). The flow Reynolds number ($Re_f$) consequently stays between 61.02 and 106.78, while the Froude number (*Fr*) between 1.249 and 3.845. The flames are buoyant dominated based on Ref [28]. The co-flow air rate is varied from 0 to 20 SLPM, where the ambient air acts as an oxidiser at 0 SLPM.

The values of $L_f$, λ, and $H_f$-*ave* of the simulated flames are compared with the experiment results, as shown in Fig. 4. The dash lines connecting the values of $L_f$, λ, and $H_f$-*ave* at each fuel and air rate are drawn to form the profiles of these parameters. All the CFD models, with the three different mesh resolutions, are shown to be capable of formulating the similar profiles of $L_f$, λ, and $H_f$-*ave* when comparing with the experimental data. The same types of flame (stable, flickering, or tip-cutting) are predicted by the fine and medium mesh models at the same fuel and co-flow air rates as the experimental result. However, the coarse mesh model predicts the flickering and stable flames at the lower co-flow air rate than those of the fine and medium mesh models. To further clarify this, the values of $L_f$ and λ approach to zero at a lower co-flow air rate than the one observed from the other mesh resolutions. The profiles of $L_f$, λ, and $H_f$-*ave* are slightly overpredicted or underpredicted by the fine and medium mesh models. This difference, however, seems to be insignificant, so both the mesh levels are capable of providing a satisfactory result. Nevertheless, the medium mesh model is selected for the further study stage, since the performance of this model was comparable to that of the fine mesh model. Also it required lower computational resources and time to process the resulting data.

## Impacts of the syngas fuel compositions

The validated CFD model (medium mesh) is now utilised to study the impacts of the syngas compositions on the occurrence of instability in the flames. At this stage, the fuel flow rate injected is varied from 0.2 to 1.4 SLPM, and combustion occurs with the ambient air as an oxidiser (i.e. the co-flow air rate is fixed to 0 SLPM). Various syngas compositions are defined to project the impacts of each species, as shown in Table 1. They are divided into two groups; (i) pure syngas ($H_2$+CO) and (ii) syngas containing other species such as $CH_4$, $CO_2$, and $N_2$. In the first group, the ratio of $H_2$:CO concentration is varied to generate the syngas fuels having a different quantity of $H_2$, e.g. 1:3 (CO-rich), 1:1 (EQ), and 3:1 ($H_2$-rich). Whereas, the ratio is kept equal (1:1) for the second group, but the percentage of the additional species ($CH_4$, $CO_2$, and $N_2$) is varied from 10% to 20%.

The Reynolds number ($Re_f$) and Froude number (*Fr*) of the fuel stream are computed according to the range of the fuel rate, $Re_f$ becomes 10–70 for hydrogen, and 22–367 for the other fuels. The value of *Fr* calculated varies between 2 and 103, but this is significantly higher than the one determined in the validation stage. Thus, the flame requires another level of analysis and in this context, 'Flame Froude number ($Fr_f$)', is introduced ([29–31]):

$$Fr_f = \frac{UY_s^{1.5}}{\left((T_{ad} - T_\infty)/T_\infty g D_f\right)^{0.5} \xi^{0.25}} \tag{13}$$

where the parameters related to the stoichiometry mixture fraction ($(Y_s)$), air/fuel density ratio ($\xi$), diameter of the fuel injector ($D_f$), adiabatic flame temperature ($T_{ad}$), velocity of fuel stream ($U$), gravitational acceleration ($g$), and ambient temperature ($T_\infty$). The flame with $Fr_f < 5$ is defined as a buoyant-dominated diffusion flame, while one with $Fr_f > 5$ is a momentum-dominated flame. $Fr_f$ calculated from all the studied fuels is significantly lower than the critical value at

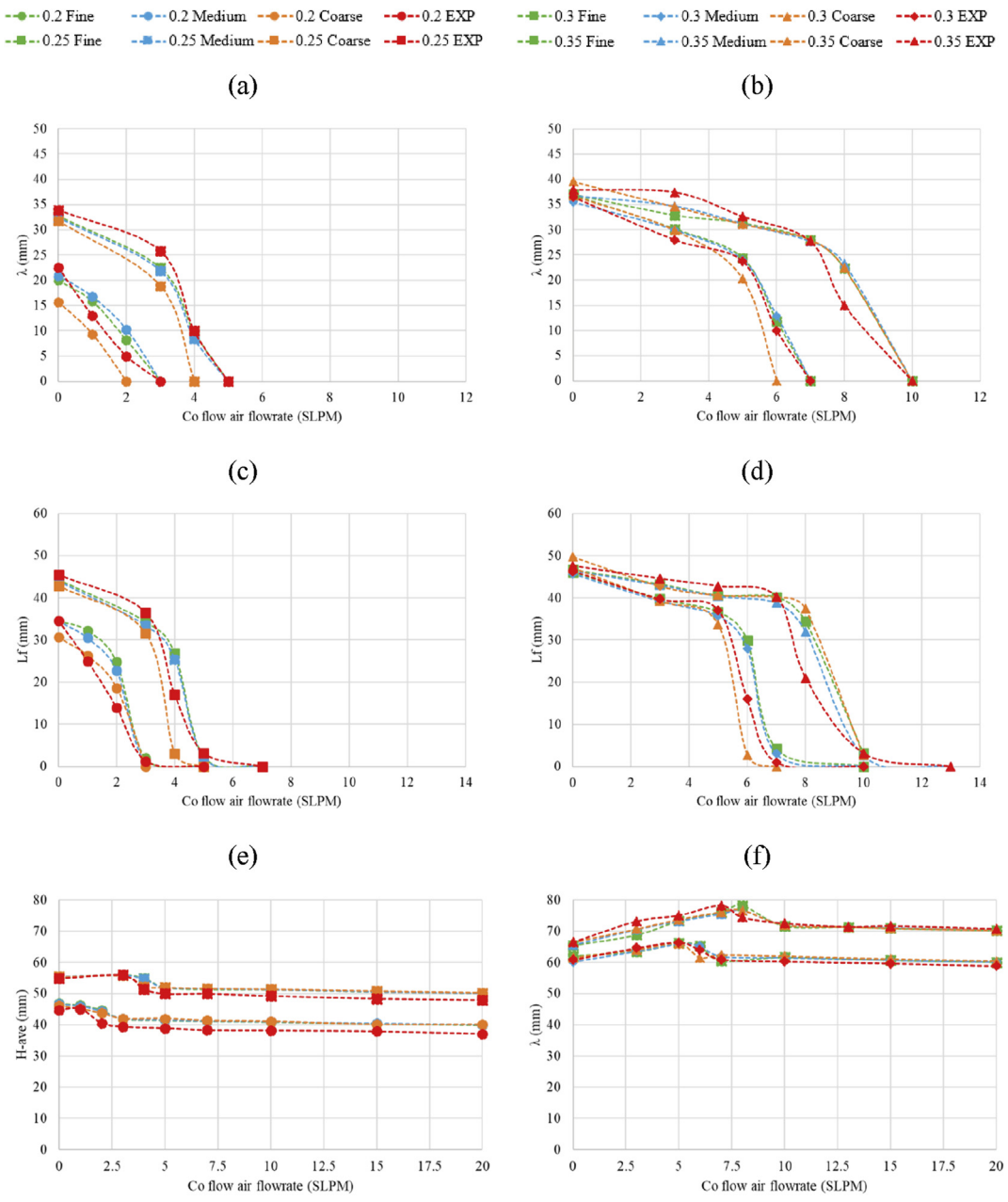


**Fig. 4 – Comparison between the experimental and CFD results: (a) and (b) the oscillation wavelength (λ), (c) and (d) the magnitude of oscillation ($L_f$), and (e) and (f) the average oscillating flame height ($H_f$-ave).**

**Table 1 – Details of the studied fuel compositions.**

| Flame types | $H_2$ | CO | $CH_4$ | $CO_2$ | $N_2$ | $H_2$:CO | Density (kg.m$^{-3}$) | Flame Froude number | Air–fuel ratio | Lower heating value (MJ/kg) |
|---|---|---|---|---|---|---|---|---|---|---|
| $H_2$ | 100% | – | – | – | – | – | 0.082 | 1.88E-3 – 1.31E-2 | 2.38 | 141.58 |
| $H_2$-rich | 75% | 25% | – | – | – | 3 | 0.348 | 1.10E-3 – 7.71E-3 | 2.38 | 33.30 |
| EQ | 50% | 50% | – | – | – | 1 | 0.614 | 4.53E-4 – 3.17E-3 | 2.38 | 18.86 |
| CO-rich | 25% | 75% | – | – | – | 0.33 | 0.878 | 4.00E-5 – 2.80E-4 | 2.38 | 13.15 |
| EQ + 10%$CH_4$ | 45% | 45% | 10% | – | – | 1 | 0.618 | 8.08E-4 – 5.65E-3 | 3.09 | 22.74 |
| EQ + 20%$CH_4$ | 40% | 40% | 20% | – | – | 1 | 0.622 | 6.27E-4 – 4.39E-3 | 3.80 | 26.58 |
| EQ + 10%$CO_2$ | 45% | 45% | – | 10% | – | 1 | 0.733 | 1.65E-3 – 1.15E-2 | 2.14 | 14.22 |
| EQ + 20%$CO_2$ | 40% | 40% | – | 20% | – | 1 | 0.851 | 2.36E-3 – 1.65E-2 | 1.90 | 10.88 |
| EQ + 10%$N_2$ | 45% | 45% | – | – | 10% | 1 | 0.667 | 1.43E-3 – 1.00E-2 | 2.14 | 15.62 |
| EQ + 20%$N_2$ | 40% | 40% | – | – | 20% | 1 | 0.720 | 1.85E-3 – 1.30E-2 | 1.90 | 12.86 |

every fuel rate and thus considered as the buoyant diffusion flame.

### *Flame characteristics and heat generation*

The temperature contour plot is initially analysed for projecting the appearance and movement of the flame during the instability cycle. At 0.2 SLPM, the stable flame is obtained from all the studied fuel compositions. The temperature contour plot representing the appearance of the stable flames of $H_2$, $H_2$-rich, EQ, and CO-rich is presented as an example in Fig. 5. While the structure of the stable flames at this fuel rate is similar, the temperature is affected by the fuel compositions. The high-temperature zone (>1800 K) is located on the mid-axis and top of the flame and due to this, the impact of fuel composition on the flame structure is weak.

However, the stable flame transforms to flickering at a relatively higher fuel rate, and the transition between the flame types occurring at a different fuel rate depends on the fuel composition. The movement and structure of the flickering flames are illustrated in Fig. 6 for $H_2$, $H_2$-rich, EQ, and CO-rich at 0.5 SLPM. As shown in the figures, the flame length increases to its maximum then drops back to the minimum value – this is typically the case occurred at all the fuel compositions. However, the flame structure is different, relying on the concentration ratio of $H_2$:CO. For example, for the flames of $H_2$ and $H_2$-rich with $H_2$:CO > 1, the position of the high-temperature area is on the flame front and above the fuel tube. While for EQ and CO-rich with $H_2$:CO $\leq$ 1, it is on the top part of the flame. The structure of the EQ syngas flames mixed with either $CH_4$, $CO_2$, or $N_2$ at 10% and 20% is also found to be the same as that of the EQ syngas, since all of them have $H_2$:CO = 1. Moreover, throughout the instability cycle, the high-temperature area expands and reduces both upward and downward along the flame front line. Also, the oscillation of the maximum flame temperature is observed; and the temperature escalates when the flame height increases.

Interesting, by increasing the fuel rate further, the flickering flame experiences a higher level of instability and subsequently becomes a tip-cutting flame. The fuel rate at which this transition occurs again strongly depends on the fuel composition, as shown in Fig. 7. For instance, the flame length escalates to its maximum value, where the tip cut occurs at the body of the flame. Following that, the flame fluctuates and consequently, its length decreases to the minimum value. The flame temperature, however, oscillates throughout the instability cycle and the high-temperature area is above the fuel tube at the beginning of the cycle. It is found that the high-temperature area is closer to the fuel tube for the flame of syngas with the higher $H_2$:CO. This area moves along the flame front line to the axis at the same level where the tip-cutting occurs. During the movement, the temperature of this area reduces, and the new high-temperature area is formed after the tip-cutting at the original position.

The average flame length ($H_f$-*ave*) of all the studied fuel compositions is compared in Fig. 8a. The profiles of $H_f$-*ave* is found to be almost linear and directly proportional to the fuel rate used. Particularly, $H_f$-*ave* is higher when the fuel rate supplied is larger, with a significant role played by the species of $CH_4$ and CO. For instance, the syngas with a lower $H_2$:CO has a higher value of $H_f$-*ave* at the same fuel rate. Also, the EQ syngas mixed with $CH_4$ has a higher $H_f$-*ave* than the EQ and EQ mixed with either $CO_2$ or $N_2$. Further, the role of $CH_4$ is stronger than CO as the profiles of EQ+10%$CH_4$ and EQ+20% $CH_4$ have a higher $H_f$-*ave* than the CO-rich case at a given fuel rate. Conversely, the higher percentage of inert $N_2$ leads to a lower value of $H_f$-*ave* as seen from the profiles of EQ+20%$N_2$ and EQ+10%$N_2$ compared to the EQ case. Having $CO_2$ in the

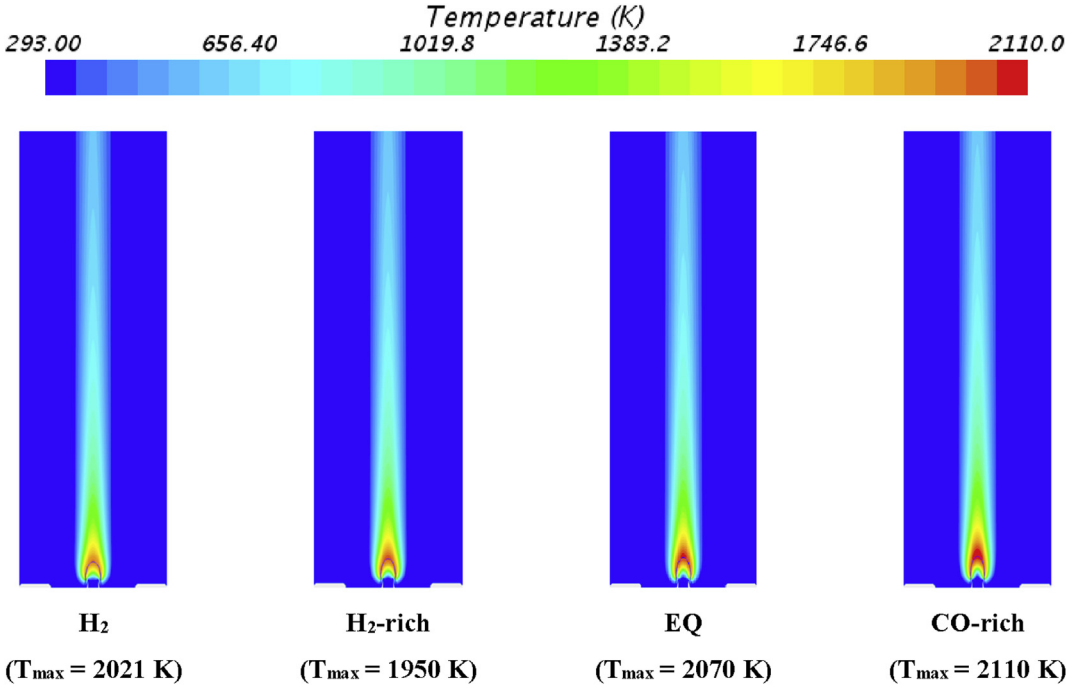


**Fig. 5 – Stable flames of $H_2$ and pure syngas ($H_2$-rich, EQ, and CO-rich) at fuel rate of 0.2 SLPM.**

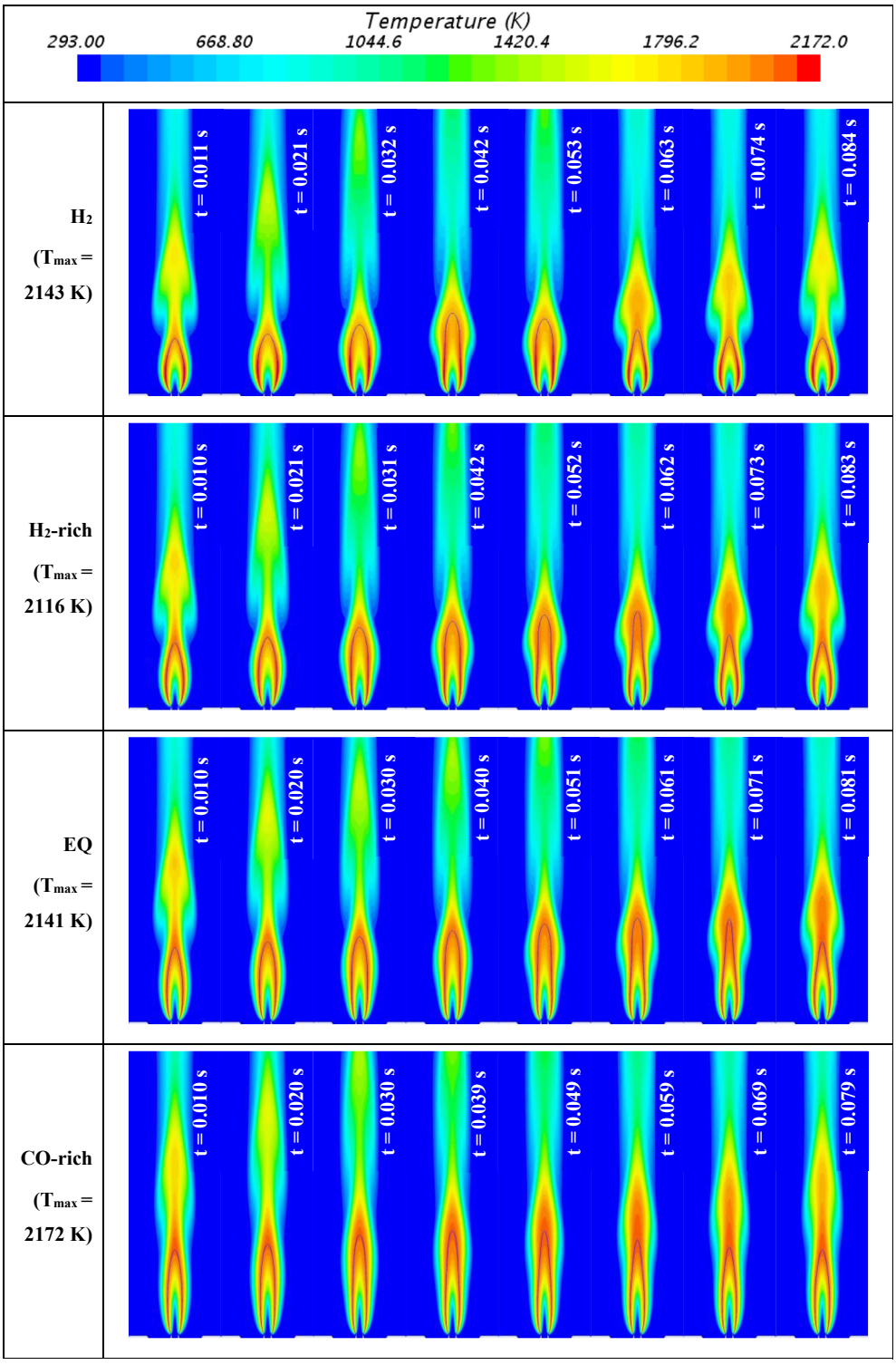


**Fig. 6 – Flickering flames of $H_2$ and pure syngas ($H_2$-rich, EQ, and CO-rich) at fuel rate of 0.5 SLPM.**

fuel composition surprisingly escalates the value of *$H_f$-ave* when the flame is unstable, as seen from the profiles of EQ+10%$CO_2$ and EQ+20%$CO_2$.

As discussed above, the flame temperature fluctuates during the instability cycle. Therefore, an average flame temperature (*T-ave*) is calculated for the different cases and presented in Fig. 8b. The profile of *T-ave*, escalates along with an increase of the fuel rate, but relies strongly on the $H_2$:CO ratio. The flames of $H_2$-rich and $H_2$ have a non-linear profile with a higher increasing rate at the lower fuel rate. On the other hand, the pattern is different for syngas having $H_2$:CO $\leq$ 1. The profile of *T-ave* of EQ, CO-rich, EQ mixed with either $CH_4$, $CO_2$, or $N_2$ are also non-linear at the fuel rate lower than 0.5 SLPM but linear at the fuel rate above. This further

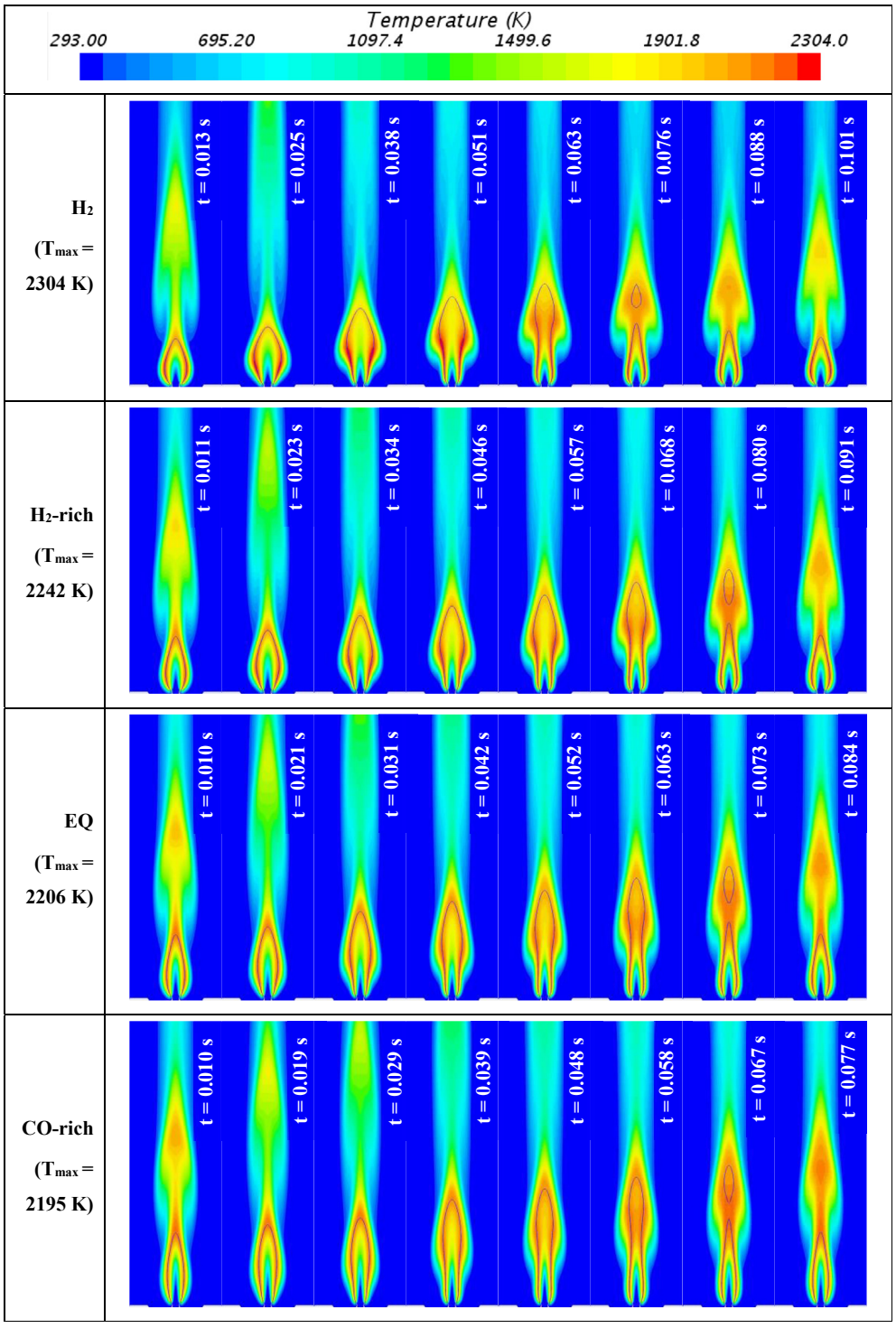


**Fig. 7 – Tip-cutting flames of $H_2$ and pure syngas ($H_2$-rich, EQ, and CO-rich) at fuel rate of 1.2 SLPM.**

implies that $H_2$ plays a significant role in the flame temperature, and the addition of $CH_4$, $CO_2$, or $N_2$ causes the reduction of *T-ave*. The impact of $CO_2$ is found to be stronger than $N_2$ and $CH_4$ at the same percentage of addition. Also, the level of impact of these species is stronger when the additional percentage of these species is higher, and the result is consistent for both the stable and unstable flames.

The total flame chemistry heat release ($Q_{total}$) is computed by combining the heat released from the chemistry reaction at every grid on the simulation domain. The average total chemistry heat release (*Q-ave*) is calculated from the maximum and minimum of $Q_{total}$, as presented in Fig. 8c. The pattern of *Q-ave* profile of all the fuel compositions is almost linear, and the higher average heat is generated at a higher fuel rate. The lower $H_2$:CO of concentration percentage and the higher concentration of $CH_4$ in fuel composition encourage the heat generation capability. The impact of $CH_4$ is stronger than CO and $H_2$. The comparable role of $CO_2$ and $N_2$

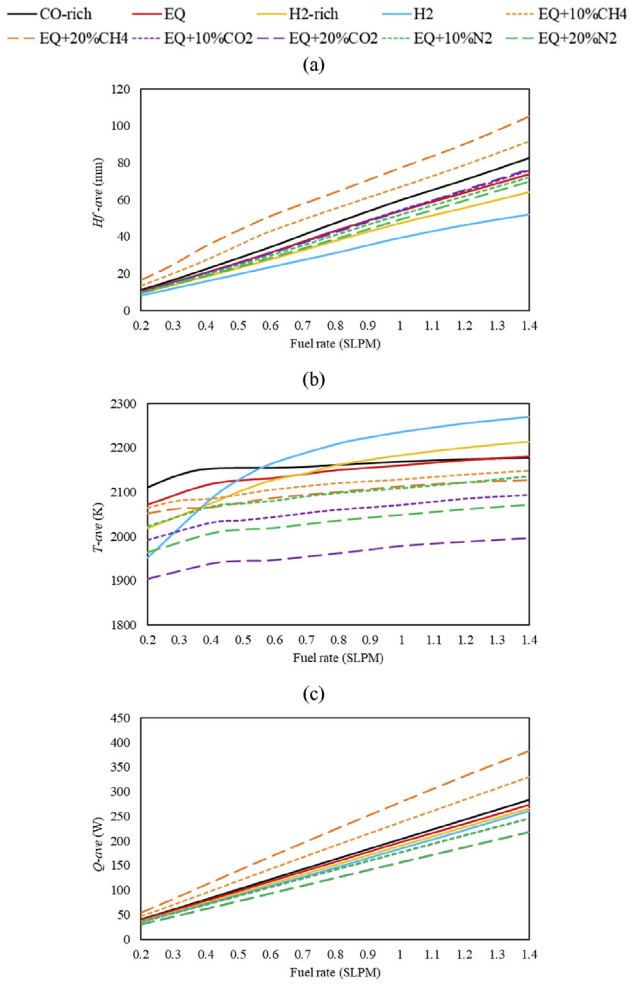


**Fig. 8 – (a) Average flame length ($H_f$-ave), (b) average flame temperature (T-ave), and (c) average total chemistry heat release (Q-ave) of all the studied fuel compositions.**

are observed as both the species cause the reduction of *Q-ave* at an equal level when they are added to syngas at the same additional percentage.

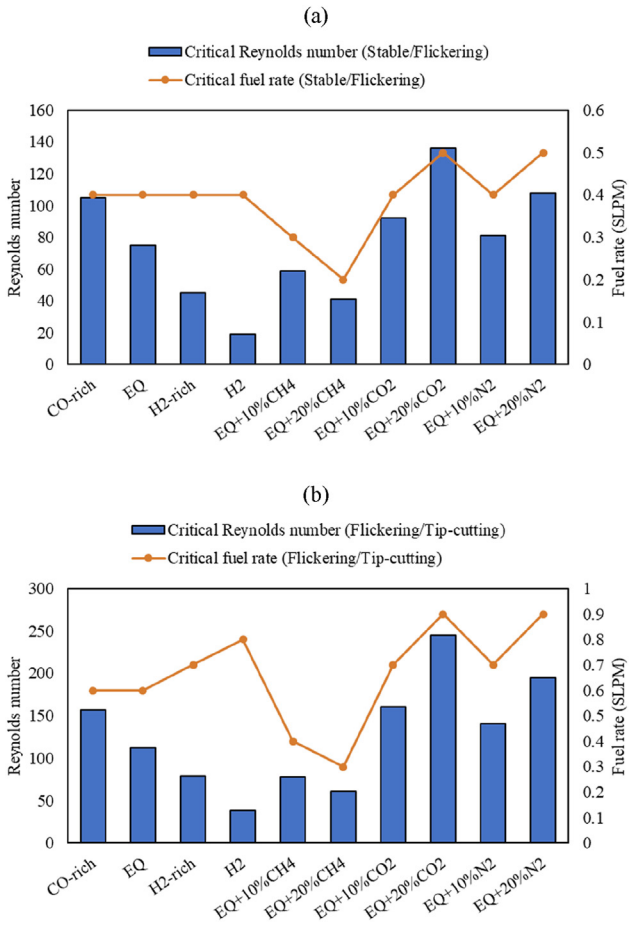


**Fig. 9 – Critical fuel rate and Reynolds number at (a) stable/flickering and (b) flickering/tip-cutting transition.**

### *Critical conditions*

The type of flame at a specific fuel and air rate identified based on the value of $L_f$ and $\lambda$, are presented in Table 2. Worth noting that the critical condition in this context refers to the transition occurring between the flame types such as stable/flickering and flickering/tip-cutting. The highest fuel rate at which a flame maintains its stable condition is also termed as a stable/flickering critical fuel rate ($\dot{v}_{s\rightarrow f}$), while the highest fuel

**Table 2 – Flame type at each fuel rate.**

| Fuel composition | Fuel rate (SLPM) | | | | | | | | | | | | |
|---|---|---|---|---|---|---|---|---|---|---|---|---|---|
| | 0.2 | 0.3 | 0.4 | 0.5 | 0.6 | 0.7 | 0.8 | 0.9 | 1 | 1.1 | 1.2 | 1.3 | 1.4 |
| $H_2$ | S | S | S | F | F | F | F | T | T | T | T | T | T |
| $H_2$-rich | S | S | S | F | F | F | T | T | T | T | T | T | T |
| EQ | S | S | S | F | F | T | T | T | T | T | T | T | T |
| CO-rich | S | S | S | F | F | T | T | T | T | T | T | T | T |
| EQ+10%$CH_4$ | S | S | F | T | T | T | T | T | T | T | T | T | T |
| EQ+20%$CH_4$ | S | F | T | T | T | T | T | T | T | T | T | T | T |
| EQ+10%$CO_2$ | S | S | S | F | F | F | T | T | T | T | T | T | T |
| EQ+20%$CO_2$ | S | S | S | S | F | F | F | F | T | T | T | T | T |
| EQ+10%$N_2$ | S | S | S | F | F | F | T | T | T | T | T | T | T |
| EQ+20%$N_2$ | S | S | S | S | F | F | F | F | T | T | T | T | T |

rate before the flickering flame transforms to tip-cutting is a flickering/tip-cutting critical fuel rate ($\dot{v}_{f\to t}$). The values of $\dot{v}_{s\to f}$ and $\dot{v}_{f\to t}$, therefore, represent the sensitivity of the flames to transform from one to another type. As such, the lower value refers to a higher sensitivity level as the smaller change in the fuel rate could change the flame type.

Further, the value of $Re_f$ at both the types of the critical fuel rate reveals the flow condition where the transition is likely to occur. Also, there are two types of critical $Re_f$ according to the type of transition: $Re_{s\to f}$ is the critical value at stable/flickering transition whereas $Re_{f\to t}$ at flickering/tip-cutting conversion. At the stable/flickering transition,$\dot{v}_{s\to f}$ and $Re_{s\to f}$ of all the studied fuel compositions are compared in Fig. 9a. The value of $\dot{v}_{s\to f}$ of CO-rich, EQ, $H_2$-rich, and $H_2$ are kept equal at 0.4 SLPM; thus, the ratio of $H_2$:CO does not affect the value of $\dot{v}_{s\to f}$ at this transition. However, the impact of $H_2$:CO on $Re_{s\to f}$ is clearly observed; as the lower ratio provides the higher value. Also, the value of $Re_{s\to f}$ of CO-rich (105) is greater than that of EQ (75), $H_2$-rich (45) and $H_2$ (19) respectively. The value of $Re_{s\to f}$ also escalates to 92 and 136 for 10% and 20% of $CO_2$, respectively, while to 81 and 108 for 10% and 20% of $N_2$, respectively. On the other hand, the value of $\dot{v}_{s\to f}$ remains at 0.4 SLPM when the species $CO_2$ or $N_2$ is mixed with EQ at 10% and increases to 0.5 SLPM when the additional percentage is 20%. The impact of $CO_2$ and $N_2$ on the sensitivity to the fuel rate are hence comparable to become a flickering flame. In contrast, diluting syngas with $CH_4$ decreases the value of $Re_{s\to f}$ and further causes a higher level of sensitivity for the stable/flickering transition.

In Fig. 9b, the flickering/tip-cutting transition is investigated and $\dot{v}_{f\to t}$ and $Re_{f\to t}$ of all the studied fuel compositions are presented. The higher $H_2$:CO escalates $\dot{v}_{f\to t}$ since the flame of $H_2$ has the higher value of this parameter (0.8 SLPM) than $H_2$-rich (0.7 SLPM), EQ (0.6 SLPM), and CO-rich (0.6 SLPM). According to this, CO increases the sensitivity level or encourages the transformation from the flickering to the tip-cutting flame when the fuel rate increases, and the effect of $H_2$ is in the opposite direction. The higher $H_2$:CO also leads to the higher $Re_{f\to t}$ as seen from a higher value of CO-rich (157) than EQ (112), $H_2$-rich (79), and $H_2$ (38), respectively. The effect of $CH_4$, $CO_2$, and $N_2$ on $\dot{v}_{f\to t}$ is in the same direction as that on $\dot{v}_{s\to f}$. That is, adding $CH_4$ to syngas reduces $\dot{v}_{f\to t}$ to 0.4 and 0.3 SLPM at 10% and 20% of additional percentage; thus, the sensitivity level in the flickering/tip-cutting transition increases. This action also decreases $Re_{f\to t}$ to 78 and 61 at 10% and 20% of additional percentage, respectively. However, diluting $CO_2$ or $N_2$ at 10% and 20% conversely reduces the sensitivity level as the value of $\dot{v}_{f\to t}$ increases to 0.7 and 0.8 SLPM. The comparable role of $CO_2$ and $N_2$ on the critical fuel rate is again emphasised, and the dilution also rises the value of $Re_{f\to t}$ to (i) 161 and 245 for 10% and 20% of $CO_2$, and (ii) 141 and 195 for 10% and 20% of $N_2$, respectively.

### *Flame instabilities*

The parameters $L_f$ and $\lambda$ express the level of flame instability and tip-cutting phenomenon. Comparing the value of $L_f$ between the flames of different fuel composition, the higher

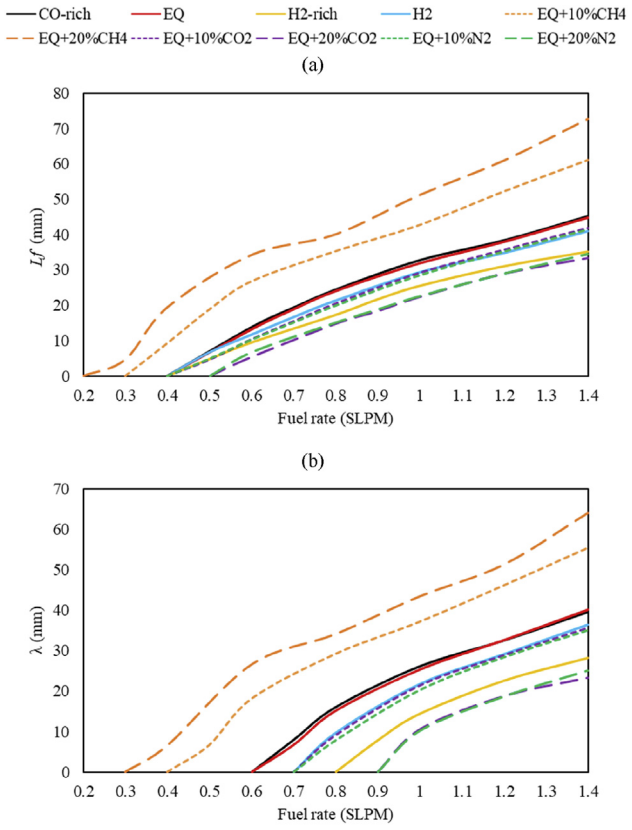


**Fig. 10 – (a) Magnitude of oscillation ($L_f$) and (b) oscillation wavelength (λ).**

value of $L_f$ represents the higher level of instability as the flame moves to the larger range. Similarly, the higher value of $\lambda$ implies the higher level of tip-cutting phenomenon since the distance between the maximum flame length and tip position is longer. For that, the profiles of $L_f$ and $\lambda$ of all the studied compositions are compared in Fig. 10a–b, and as seen the profile pattern of these parameters is similar for all the fuel compositions. Also, they are directly proportional to the fuel rate and it is reported that the higher level of instability and tip-cutting phenomenon escalate at a higher fuel rate. Specifically, the value of $L_f$ is found to be above zero at the fuel rate higher than $\dot{v}_{s\to f}$. Similarly, $\lambda > 0$ at the fuel rate higher than that of $\dot{v}_{f\to t}$. Nevertheless, the values of $L_f$ and $\lambda$ of each fuel composition are different at the same fuel rate, and this finding, therefore, further reveals the impact of diversity in the fuel composition of syngas/producer gas on these parameters. The results again emphasise the comparable role of $CO_2$ and $N_2$, while an addition of species $CH_4$ significantly increases the level of instability and tip-cutting phenomenon.

Furthermore, the frequency range also relies directly on the fuel composition, as shown in Fig. 11a–b. More specifically, a higher $H_2$:CO ratio in the syngas composition affects the lower frequency at the same fuel rate. The range is 12.5–13.2 Hz for CO-rich, which is higher than the one obtained from EQ (11.8)-(12.3) Hz), $H_2$-rich syngas (10.8–12 Hz) and $H_2$ (9.6–11.8 Hz). The flame of EQ mixed with $CO_2$ has a higher F than EQ mixed with $N_2$ or $CH_4$ at the same additional

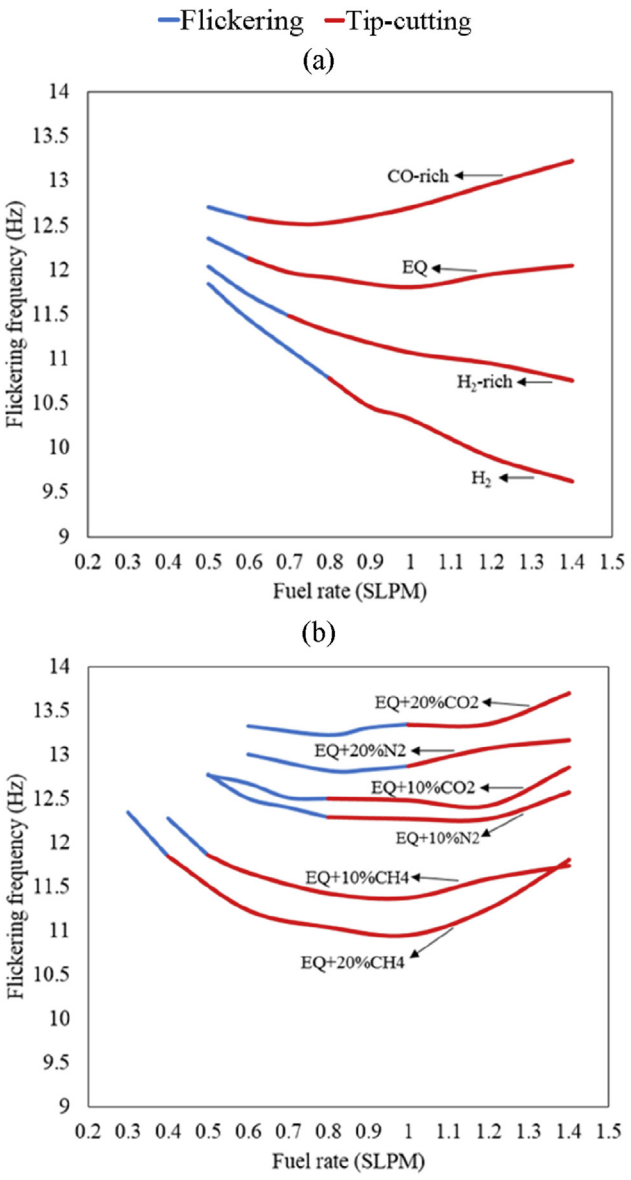


**Fig. 11 – Flickering frequency (F) of all the studied syngas compositions.**

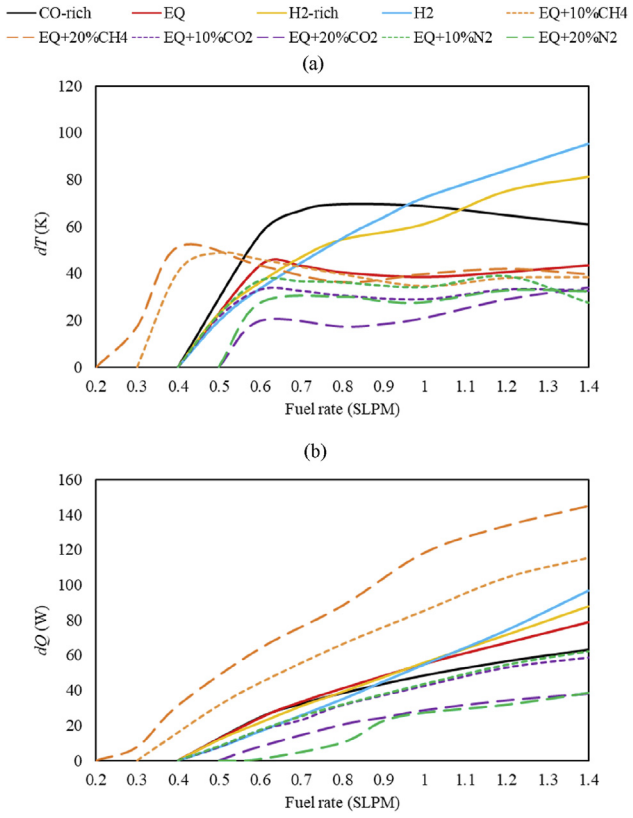


**Fig. 12 – Fluctuation of (a) average flame temperature (dT) and (b) average total chemistry heat release (dQ).**

percentage and fuel rate supplied into combustion. The frequency range of EQ mixed with $CH_4$ is 10.9–12.3 Hz, EQ mixed with $CO_2$ is 12.5–13.7 Hz, and EQ mixed with $N_2$ is 12.3–13.2 Hz. By comparing the range of *F*, the addition of $CO_2$ and $N_2$ rises the value of *F*, but an opposite direction is found for the addition of $CH_4$.

### *Fluctuation of flame temperature and heat release*

The fluctuations of the flame temperature (*dT*) and total chemistry heat release (*dQ*) compared in Fig. 12a–b are affected directly by the level of flame instability reported above. Similar to the profiles of average flame temperature (*T-ave*), *dT* relies strongly on $H_2$:CO and becomes prominent for the flames of $H_2$-rich ($H_2$:CO > 1) and $H_2$. This is also influenced by the fuel rate as seen for the $H_2$-rich flames when the fuel rate >8 SLPM. However, for the CO-rich flame ($H_2$:CO < 1), its magnitude drops but escalates again for the syngas flame having $H_2$:CO = 1. More specifically, in terms of a quantitative comparison, at the maximum studied fuel rate (i.e. 1.4 SLPM), the $H_2$ flame has the highest *dT* (95 K) followed by the $H_2$-rich (81 K), CO-rich (61 K), and syngas (27–40 K) flames. Consequently, a conclusion could be drawn for this that $H_2$ playing an important role in destabilising the flame temperature.

The impacts of other species on *dQ* are also illustrated as it is reported that $CH_4$ significantly increases the fluctuation level in the heat generation capability, since the *dQ* profiles of EQ mixed with $CH_4$ is clearly above of the other fuel compositions. The role of $CO_2$ and $N_2$ are again comparable; as the value of *dQ* of EQ mixed with either $CO_2$ or $N_2$ is similar at the same additional percentage. Both the species reduce the fluctuation in the heat generation capability since the profile of EQ mixed with either of these species is below the profile of EQ. Again, at the maximum studied fuel rate (1.4 SLPM), the flame of EQ+20%$CH_4$ has the highest level of fluctuation (145 W) followed by EQ+10%$CH_4$ (116 W) and $H_2$ (91 W) respectively. The lowest level is observed from EQ mixed with either $CO_2$ or $N_2$ at 20% as ~39 W.

### *Optimum heat generation*

For an unstable flame, the values of *Q-ave* and *T-ave* are the average value without consideration of any instability. Thus, it is unreasonable to conclude that the higher value of these parameters would refer to the higher heat generation capability since they do not consider any fluctuation of the total

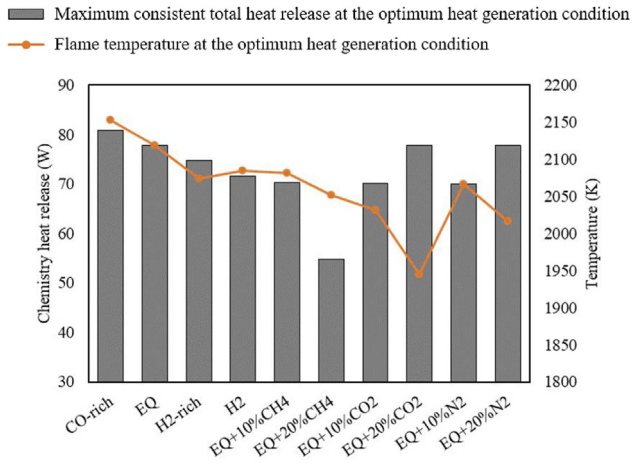


**Fig. 13 – Total heat release and flame temperature at the optimum heat generation condition.**

chemistry heat release ($dQ$) and the flame temperature ($dT$). Therefore, the flame having a lower value of $dQ$ and $dT$, but with higher $Q$-*ave* is preferable. By this perception, the combustion condition that provides the maximum consistency heat ($dQ = 0$ and $dT = 0$) is thus the optimum heat generation condition. This condition also refers to $Q$-*ave* at the stable/flickering critical fuel rate ($\dot{v}_{s\rightarrow f}$). The comparison of $Q$-*ave* at this condition of all the studied fuel compositions is shown in Fig. 13. Additionally, the flame temperature ($T$-*ave*) at this condition is also presented along with $Q$-*ave* in this figure.

The highest optimum heat generation is reported by the CO-rich flame as 81 W at the flame temperature of 2153 K. This result is subsequently followed by the heat released from the flames of EQ, EQ+20%$CO_2$, and EQ+20%$N_2$. At this condition, the respective temperature of flame is 2118 K, 1945 K, and 2016 K. Consequently, the species such as CO, $CO_2$, and $N_2$ encourage the higher optimum heat generation of syngas. The value of $\dot{v}_{s\rightarrow f}$ also represents the consumption of fuel for the optimum heat generation condition. The consumption of both CO-rich and EQ are 0.4 SLPM, while it is 0.5 SLPM for EQ+20% $CO_2$, and EQ+20%$N_2$. The lower consumption for the same amount of heat is the benefit of having CO in the syngas composition. In contrast, the flame of EQ+20%$CH_4$ has the lowest optimum heat generation (55 W at 2052 K) so adding $CH_4$ to syngas has a negative impact on the consistent heat generation.

## Discussion

The stable, flickering and tip-cutting flames of syngas with various fuel compositions are formulated to project the impacts of fuel composition on the occurrence of flame instability. The key findings, especially considering the roles of each species obtained from the analysis are discussed below:The reaction mechanism selected is allowed the analysis of an impact of each species in the syngas composition. The studied fuel composition has single and multiple combustible species such as $H_2$, CO and $CH_4$, which have different reaction rate. The results obtained from the fuel having different volume fraction of these species are then expected to be different.

Both $H_2$ and CO, which are the two major species in the syngas fuel composition, play a significant role in various aspects. For example, the analysis showed the advantage of having a higher concentration of CO over $H_2$ in the syngas composition. Though syngas with a lower $H_2$:CO has a higher level of instability, the level has an upper limit when $H_2$:CO = 1. In addition, syngas with a lower $H_2$:CO has a higher average total chemistry heat release with low fluctuation in the heat generation (lower $dQ$). With regard to $CH_4$, it has a negative impact on the flame instability, but CO is the most desirable among the combustible species in the syngas composition. However, this finding is obtained by considering only the heat generation capability and flame instability and is, therefore, not included in the emission formation. On the other hand, $H_2$ plays a significant role in increasing the average flame temperature (higher $T$-*ave*) and consequently, encourages the fluctuation of this parameter.

For a stable diffusion flame, the higher concentration of $CH_4$ in the syngas composition is suggested since this species enhances the heat generation capability of the flame and also lowers the emission formation [20]. In an unstable flame, however, this species promotes the level of instability as well as the fluctuation in heat generation. Also, further adding $CH_4$ to the syngas gas composition raises the level so the flame becomes unstable when the fuel rate increases. Therefore, it is less desirable among the combustible species in the syngas composition when the oxidiser supplied into combustion is limited and the flame is unstable. The sufficient rate of oxidiser stream is necessary to maintain the flame stability and to potentially utilise the benefit of $CH_4$ on the heat generation capability effectively.

As a non-combustible species, the higher concentration of $CO_2$ and $N_2$ in the syngas composition decreases the capability in heat generation. Nevertheless, an addition of these species into the syngas composition has a benefit in the reduction of instability level and fluctuation in heat generation. Furthermore, the result points to the comparable role of $CO_2$ and $N_2$ on various aspects, e.g. the flame instability level ($L_f$), the average total chemistry heat release ($Q$-*ave*), and the fluctuation in heat generation ($dQ$). Diluting either of these species into the syngas composition is one of the options which could increase the flame stability. Nevertheless, this method requires further analysis for optimising the proper additional percentage, which balances between the reduced heat generation capability and the increased stability level.

The study result obtained in this work could also be compared with the study of [20] where the stable flame of syngas/producer gas is investigated extensively on various aspects. It is found that the effect of $H_2$, CO, $CH_4$, $CO_2$ and $N_2$ on the flame length, flame temperature and heat generation are in the same direction for the stable and unstable flames. The exception is observed only from the impact of $CO_2$ on the flame length. The higher concentration of this species results in the reduction of flame length ($H_f$) for a stable flame but increases the average flame length ($H_{f\text{-}ave}$) in an unstable flame. The result in this work also emphasises the finding of [20] for the relation between $Q$-*ave* and $T$-*ave*. The flame generating

the higher *Q-ave* is not necessary to have a *T-ave*. For instance, the flame of EQ+20%$CH_4$ generates a higher *Q-ave* than CO-rich syngas at every fuel rate although its profile of *T-ave* is lower. As a result, the direction of the result found from the stable flame is also valid for the unstable flame.

All the studied flames are formulated from the same fuel rate (same velocity) and diameter of the fuel injector. Therefore, the critical Reynolds numbers for both the types of transition (e.g. $Re_{s\to f}$ and $Re_{f\to t}$) rely strongly on the fluid property (e.g. dynamic viscosity and density) according to the definition of $Re_{s\to f}$ and $Re_{f\to t}$.

The simulation is processed on the axisymmetric domain. Thus, the impact of possible three-dimension vortex interactions e.g. vortex stretching which could lead to the extended computed flame is excluded. However, this limitation does not play a significant role since the laminar flow is studied in this work.

Lastly, further study is suggested for the impact of syngas composition on the elimination of flame instability by supplying a larger amount of oxidiser. The different instability level of the flame of various syngas composition would demand a different amount of oxidiser to eliminate. The impact of each species in syngas composition on this aspect is significant, and the result could be the guideline for reducing and eliminating the flame instability on various combustion applications.

## Conclusion

A CFD model was formulated for studying the impacts of the diversity in the syngas composition on the occurrence of the flame instability in a laminar co-flow diffusion flame. The stable flame was observed at a low fuel rate which, however, transformed to a flickering and tip-cutting flame respectively at a higher fuel rate. The effect of species in the syngas composition on this phenomenon was also examined and the key conclusion is as follows:

- Syngas with a lower ratio of $H_2$:CO has a higher level of instability; nevertheless, the level does not rise further when the ratio is lower than 1. Adding $CH_4$ to syngas significantly increased the instability level, and the flame was more sensitive to the fuel rate. The opposite was found when syngas was diluted with $CO_2$ and $N_2$.
- $CH_4$ and CO concentrations in syngas have a significant impact on the increase of heat generation capability. $CH_4$ has a stronger role than CO in this aspect; however, higher concentration of $CH_4$ in the fuel composition also promotes the fluctuation in the heat generation significantly. This suggests that CO is preferable than $CH_4$ as the higher concentration of CO in syngas could reduce the level of heat generation fluctuation.
- The effect of $H_2$ on the increase of flame temperature was significant, and this species also encouraged the fluctuation level of flame temperature.
- The effect of $H_2$, CO, $CH_4$, $CO_2$ and $N_2$ on the flame length, temperature, and heat generation was mostly in the same direction for the stable and unstable flames. An exception was obtained from the effect of $CO_2$ on the flame length. The higher concentration of this species reduced the flame length ($H_f$) in the stable flame but increased the average flame length ($H_{f\text{-}ave}$) for the unstable flame.

Finally, a diffusion flame, as an energy source, and also the development of production process of syngas for high-performance fuel composition, provide a higher level of flame stability and heat generation. Therefore, it is anticipated that the results presented in the paper have the potential benefit in the effective design of a combustion system for the utilisation of syngas and hydrogen fuels.

## Declaration of competing interest

The authors declare that they have no known competing financial interests or personal relationships that could have appeared to influence the work reported in this paper.

## Acknowledgement

The first author would like to thank the Royal Thai Navy for funding his postgraduate research study at the University of Glasgow. The content of the paper is based on the first author's PhD thesis available at the University of Glasgow's repository [32]. The second author also acknowledges EPSRC (EP/N020472/1) and The RAEng/Leverhulme Trust Senior Research Fellowship (LTSRF1718\14\45) support.

## REFERENCES

[1] Gohari Darabkhani H, Wang Q, Chen L, Zhang Y. Impact of co-flow air on buoyant diffusion flames flicker. Energy Convers Manag 2011;52(8–9):2996–3003.
[2] Ellabban O, Abu-Rub H, Blaabjerg F. Renewable energy resources: current status, future prospects and their enabling technology. Renew Sustain Energy Rev 2014;39:748–64.
[3] Lozano F, Lozano R. Assessing the potential sustainability benefits of agricultural residues:Biomass conversion to syngas for energy generation or to chemicals. J Clean Prod 2018;172:4162–9.
[4] Mackaluso JD. The use of syngas derived from biomass and waste products. MMG 445 Basic Biotechnology eJournal 2007;3:98–103.
[5] Sepe AM, Li J, Paul MC. Assessing biomass steam gasification technologies using a multi-purpose model. Energy Convers Manag 2016;129:216–26.
[6] Basu P. Biomass gasification, pyrolysis, and torrefaction practical design and theory. 2nd ed. Amsterdam: Academic Press; 2013.
[7] Sutardi T, Paul MC, Karimi N. Investigation of coal particle gasification processes with application leading to underground coal gasification. Fuel 2019;237:1186–202.
[8] Sutardi T, Paul MC, Karimi N, Younger PL. Numerical modelling for process investigation of a single coal particle combustion and gasification. In: World Congress on engineering 2017. London: WCE 2017); 2017. p. 946–51.
[9] Salem AM, Paul MC. An integrated kinetic model for downdraft gasifier based on a novel approach that optimises

the reduction zone of gasifier. Biomass Bioenergy 2018;109:172–81.
[10] Salem AM, Kumar U, Izaharuddin AN, Dhami H, Sutardi T, Paul MC. Advanced numerical methods for the assessment of integrated gasification and CHP generation technologies. In: Coal and biomass gasification. Singapore: Springer; 2018. p. 307–30.
[11] Chanphavong L, Zainal ZA. Characterization and challenge of development of producer gas fuel combustor: a review. J Energy Inst 2018:1–14.
[12] Ranga Dinesh K, Jiang X, Kirkpatrick M, Malalasekera W. Combustion characteristics of H2/N2 and H2/CO syngas nonpremixed flames. Int J Hydrogen Energy 2012;37(21):16186–200.
[13] Dinesh KR, Jiang X, Oijen JV. Direct numerical simulation of non-premixed syngas burning with detailed chemistry. Fuel 2013;107:343–55.
[14] Swarnkar P, Sahu AK, Sundararajan T. Numerical study of effect of hydrogen content on the structure of syngas diffusion flame. In: 10th international Conference on heat transfer. Orlando, Florida: Fluid Mechanics and Thermodynamics; 2014. p. 704–13.
[15] Piemsinlapakunchon T, Paul MC. Characterisation of syngas laminar diffusion flame with an effect of its varying composition. In: World Congress on engineering 2017; 2017. London, UK.
[16] Piemsinlapakunchon T, Paul MC. Effects of content of hydrogen on the characteristics of co-flow laminar diffusion flame of hydrogen/nitrogen mixture in various flow conditions. Int J Hydrogen Energy 2018;43(5):3015–33.
[17] Xi J, Yuan Y, Gu Z, Yang W, Zhang X, Wang S. Effect of CO2/N2/CH4 dilution on NO formation in laminar coflow syngas diffusion flames. Energy Sources 2018;40(7):821–9.
[18] Xu H, Liu F, Sun S, Zhao Y, Meng S, Tang W. Effects of H 2 O and CO 2 diluted oxidizer on the structure and shape of laminar coflow syngas diffusion flames. Combust Flame 2017;117:67–8.
[19] Molino A, Larocca V, Chianese S, Musmarra D. Biofuels production by biomass gasification. Energies 2018;11(811):1–31.
[20] Piemsinlapakunchon T, Paul MC. Effects of fuel compositions on the heat generation and emission of syngas/producer gas laminar diffusion flame. Int J Hydrogen Energy 2019;44(33):18505–16.
[21] Darabkhani HG, Zhang Y. Stabilisation mechanism of a flickering methane diffusion flame with co-flow of air. Eng Lett 2010;18(4):2–8.
[22] Klein SA, Alvarado FL. Engineering equation solver (EES) user manual, vol. 53562. Middleton, WI: F-Chart Software; 1999. 4406 Fox Bluff Rd.
[23] Mathur S, Saxena S. Methods of calculating thermal conductivity of binary mixtures involving polyatomic gases. Appl Sci Res 1967;17:155–68.
[24] cd-adapco. STAR CCM+ version 11 User guide," Cd-adapco. 2016 [Online]. Available: https://stevedocs.cd-adapco.com/starccmplus_latest_en/index.html?param=eNUMK.
[25] A. Kazakov and M. Frenklach, "Reduced Reaction Sets based on GRI-Mech 1.2," [Online]. Available: http://combustion.berkeley.edu/drm/. [Accessed 4 12 2017].
[26] Fischer M, Jiang X. An assessment of chemical kinetics for bio-syngas combustion. Fuel 2014;137:293–305.
[27] Cohen SD, Hindmarsh AC. CVODE, A stiff/Nonstiff ODE solver in C. Comput Phys 1996;10(2):138–43.
[28] Drysdale D. An introduction to fire dynamics. New York: JOHN WILEY & SONS; 2011.
[29] Delichatsios MA. Transition from momentum to buoyancy-controlled turbulent jet diffusion flames and flame height relationships. Combust Flame 1993;92(4):349–64.
[30] Bahadori MY, Stocker DP, Vaughan DF, Zhou L, Edelman RB. Effects of buoyancy on laminar, transitional and turbulent gas jet diffusion flames. In: Modern developments in energy, combustion and spectroscopy. New York: Pergamon Press; 1993. p. 49–66.
[31] Choudhuri AR, Gollahalli SR. Characteristics of hydrogen-hydrocarbon composite fuel turbulent jet flames. Int J Hydrogen Energy 2003;28(4):445–54.
[32] Piemsinlapakunchon T. Impact of diversity in syngas/producer gas composition on stable and unstable laminar diffusion flames. Glasgow: University of Glasgow; 2019. PhD Thesis, http://theses.gla.ac.uk/76711/.

## Nomenclature

*Uppercase letters*

$C_v$: Contribution to the molar specific heat of each species
CCN: Convective courant number
D: Diffusivity ($m^2$ kmol/J.s)
$D_f$: Diameter of fuel injector (m)
E: Total energy (J)
F: Flickering frequency (Hz)
Fr: Froude number
$Fr_f$: Flame Froude number
$H_f$: Flame height (m)
J: Diffusive flux (mol $m^{-2}$ $s^{-1}$)
$L_f$: Magnitude of oscillation (m)
Q: Thermal energy production rate ($J/m^3$-s)
Q: Chemistry heat release (W)
R: Production rate of species (mol/s)
Re: Reynolds number
S: Optical path length (m)
T: Temperature (K)
Y: Mass fraction of species
$Y_s$: Stoichiometry mixture fraction
U: Velocity of fuel stream (m/s)

*Greek letters*

$\rho$: Fluid density ($kg/m^3$)
$\mu$: Dynamic viscosity (Pa-s)
$\lambda$: Oscillation wavelength (m)
$\lambda t$: Thermal conductivity (W/m-k)
$\xi$: Air/fuel density ratio

*Lowercase letters*

g: Gravitational acceleration ($m/s^2$)
h: Specific enthalpy (J)
p: Pressure (Pa)
q: Energy flux ($W/m^2$)
t: Time (s)
u: Velocity component (m/s)

*Subscripts*

ad: Adiabatic
i: Species i

$j$: Species $j$
r: Radial coordinate
x: Axial coordinate
tran: Translation
rot: Rotation
vib: Vibration
ave: Average
mix: Combination of specified parameter
$\infty$: ambient condition